1

# Quench Protection of a 16 T Block-coil Dipole Magnet for a 100 TeV Hadron Collider Using CLIQ

E. Ravaioli, J. Blomberg Ghini, V.I. Datskov, G. Kirby, M. Maciejewski, G. Sabbi, H.H.J. ten Kate, and A.P. Verweij

***Abstract*—Protection against the effects of a quench is a crucial challenge for 16 T class superconducting dipole magnets for a future 100 TeV Hadron collider. To avoid damage due to overheating of the coil's hot-spot, the heat generated during the quench has to be homogeneously distributed in the winding pack by quickly and uniformly transferring to the normal state voluminous coil sections. Conventional protection systems rely on quench heaters placed on the outer surfaces of the coils. However, this technique has to confront significant challenges in order to achieve the fast transitions required by high magnetic-field magnets. The recently-developed Coupling-Loss-Induced Quench (CLIQ) utilizes inter-filament coupling loss as an effective intra-wire heat deposition mechanism, which in principle is faster than thermal diffusion. Furthermore, the CLIQ technology is based on simple and robust electrical components in contact with the coil only in a limited number of easily accessible and well-insulated points. Hence, expected occurrence of failure and electrical breakdown is significantly reduced. As a case study, the design of a CLIQ-based protection system for a 14 meter long, 16 T, $Nb_3Sn$ block-coil dipole magnet is demonstrated here. Various magnet design features can be adjusted for improving CLIQ performance and optimize its integration in the magnet system. CLIQ provides future magnet designers with a solution for a very effective, yet electrically robust, quench protection system, resulting in better magnet performance and lower cost than would be possible with a traditional approach to magnet protection.**

***Index Terms*—accelerator magnet, CLIQ, magnet design, quench protection, superconducting coil.**

## I. Introduction

VARIOUS studies have been carried out aimed at designing particle accelerators achieving collision energies significantly beyond the LHC [1]–[5]. In particular, CERN launched a Future Circular Collider (FCC) study aiming at a 100 TeV collision energy using 16 T dipole magnets [6]–[9].

$Nb_3Sn$ magnets are currently selected as the baseline technology, and block-coil geometries are considered as a promising approach for this application [10]–[12]. The HD2 coil design [10], [13]–[18], shown in Fig. 1, will be used as a reference for the analysis and be hereafter referred to as "Coil A". The magnet and conductor parameters, based on design calculations and test results of dipole models, are summarized in Table I [10]. This coil generates a dipole magnetic field $B_d$=16 T with a transport current of about 18.6 kA. Coil A represents a design already manufactured various times in the past years, successfully tested, and based on a proven conductor.

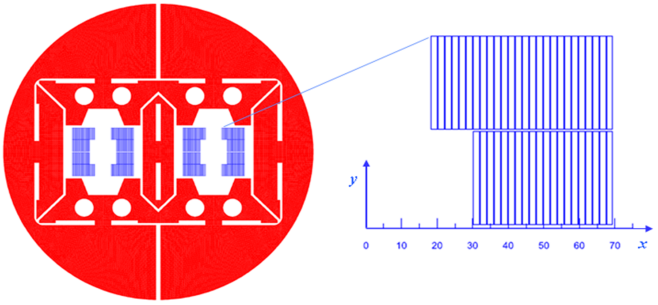


Fig. 1. Cross-section of the 16 T block-coil dipole magnet (Coil A) [10].

TABLE I
Reference Magnet and Conductor Parameters [10].

| Parameter | Unit | Value |
|---|---|---|
| Nominal current, $I_{\mathrm{nom}}$ | kA | 18.6 |
| Dipole field at $I_{\mathrm{nom}}$ | T | 16.0 |
| Peak field in the cable at $I_{\mathrm{nom}}$, $B$ | T | 16.9 |
| Operating temperature, $T$ | K | 1.9 |
| Differential inductance at $I_{\mathrm{nom}}$ | mH | 2×69 |
| Stored energy at $I_{\mathrm{nom}}$ | MJ | 2×48 |
| Magnetic length | m | 14.0 |
| Number of turns per pole | - | 54 |
| Number of strands | - | 51 |
| Strand diameter | mm | 0.8 |
| Bare cable width | mm | 22.0 |
| Bare cable thickness | mm | 1.40 |
| Insulation thickness | mm | 0.10 |
| Fraction of non-Copper | - | 0.55 |
| Critical current density ($T$=1.9 K, $B$=16 T) | kA/mm$^2$ | 2.14 |
| Filament twist pitch | mm | 14 |
| RRR of the copper matrix (measured) | - | 287 |

Due to the very high energy density of this design, the protection of this high magnetic-field coil is very challenging if the winging pack has to absorb the magnet's stored energy. Past studies showed that protection systems based on conventional quench heaters may require a substantial increase of the fraction of copper in the conductor in order to maintain the coil's hot-spot temperature below acceptable limits [8], [10]. However, such a modification to the superconductor

E. Ravaioli and H.H.J. ten Kate are with CERN, Switzerland, and with the University of Twente, Enschede, The Netherlands. (e-mail: Emmanuele.Ravaioli@cern.ch).

G. Kirby and A.P. Verweij are with CERN, Switzerland.

J. Blomberg Ghini is with CERN, Switzerland, and with the Norwegian University of Science and Technology, Trondheim, Norway.

V.I. Datskov was with CERN, Switzerland. He is now with GSI Helmholtzzentrum für Schwerionenforschung, Darmstadt, Germany.

M. Maciejewski is with CERN, Switzerland, and with Institute of Automatic Control, Technical University of Łódź, 18/22 Stefanowskiego St., Poland.

G. Sabbi is with Lawrence Berkeley National Laboratory, Berkeley, USA.

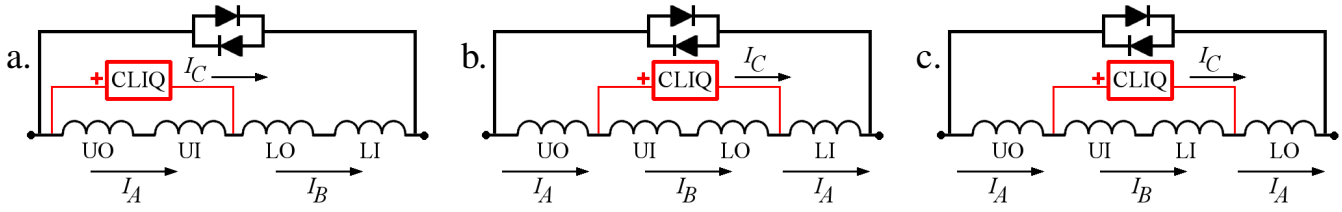


Fig. 2. Electrical schemes of alternative CLIQ configurations applied to one aperture of a two-layer dipole magnet. a. Pole-Pole. b. Crossed-Layer. c. Layer-Layer. Configuration Reverse-Layer-Layer is obtained by inverting the polarity of the CLIQ unit in the Layer Layer configuration. Each inductor represents an outer (O) or inner (I) layer of the upper (U) or lower (L) pole.

would considerably reduce the quench margin, which is already limited. Thus, a faster quench heating system is required that can quickly transfer a large portion of the coil winding pack to the normal state, thereby shortening as much as possible the discharge of the transport current.

CLIQ (Coupling-Loss Induced Quench system) is a new quench protection method recently developed at CERN [19]–[21]. It provides an electrically robust and very effective protection system, which relies on the generation of inter-filament coupling loss in the matrix of the strands. CLIQ technology has reached a high level of maturity. In the past few years, it was successfully tested on coils of different sizes, geometries (solenoid, cos-$\theta$ quadrupole and dipole), and superconductor types (Nb-Ti, $Nb_3Sn$) [21]–[27].

The use of CLIQ for protection of a full-scale, 14 m long, 16 T, block-coil dipole magnet for a Future Circular Collider, already proposed in [11], [19], [28], is here further investigated. Various CLIQ-based protection configurations are presented and analyzed with TALES (Transient Analysis with Lumped-Elements of Superconductors), a new software developed for quench-protection studies [19], [29]–[31]. The performances of CLIQ protection systems in terms of hot-spot temperature and peak characteristic voltages are investigated.

Alternative coil designs based on a modification of the number of turns, conductor properties, coil grading, and aperture size are considered in order to identify the most performing and cost-effective design.

## II. CLIQ Applied to a Block-Coil Dipole Magnet

The full description of the CLIQ system is presented in [19]. It consists of a capacitor bank with capacitance $C$ [F] charged to a voltage $U_0$ [V] and connected to the coil to protect via dedicated terminals. An example of the implementation of this method on one aperture of a two-layer dipole magnet is shown in Fig. 2a. The coil is effectively subdivided into two sections, A and B. After quench detection, the CLIQ system is activated to discharge an oscillating current $I_C$ [A], which introduces fast changes of the currents flowing in the two sections, $I_A$ and $I_B$ [A]. The resulting fast changes of the local magnetic field generate high inter-filament coupling loss [32], which is heat deposited directly in the strand matrix. In principle, this heating mechanism is much faster than thermal diffusion across insulation layers, upon which the conventional quench-heater-based technology relies.

### A. CLIQ configurations

The CLIQ performance is significantly influenced by the electrical order of the coil sections and the positioning of the CLIQ terminals [19], [25]. The electrical schemes of three alternative CLIQ configurations applied to one aperture of a two-layer dipole magnet are shown in Fig. 2. The polarities of the current changes and the directions of the magnetic-field changes introduced by these configurations in the sections of a block-coil dipole magnet are shown in Fig. 3 [19], [28].

The Pole-Pole configuration (see Fig. 2a and 3a), by which opposite current changes are introduced in the windings of the two poles, can be obtained installing one CLIQ terminal at the joint between the poles. The other configurations require inter-layer terminals, which are less easy to connect to the coil; a convenient manufacturing solution is explained in [11]. The Crossed-Layer configuration (see Fig. 2b and 3b) introduces opposite current changes in every two adjacent layers. Finally, the Layer-Layer (see Fig. 2c and 3c) introduces opposite current changes in the outer and inner layers. By changing the polarity of the CLIQ charging voltage, it is possible to introduce the first positive current pulse either in the inner (Layer-Layer) or in the outer layers (Reverse-Layer-Layer).

Configurations including intra-layer terminals characteristically achieve higher deposited power density than Pole-Pole. In fact, introducing opposite current changes in coil sections which are physically adjacent reduces the equivalent impedance of the discharge system and profits from an effective superposition of the magnetic-field changes generated by the coil sections.

### B. CLIQ discharge

The results of the simulation of a magnet discharge obtained by triggering a 100 mF, 1 kV Pole-Pole CLIQ system connected to one aperture of the magnet is shown in Fig. 4. The 3 kA, 10 Hz oscillating current introduced by CLIQ generates sufficient coupling loss to quickly transfer to the normal state voluminous regions of the winding pack. The transition to the normal state is initiated in less than 5 ms, and in about 60 ms the entire winding pack is normalized. As a result, an electrical resistance is rapidly developed in the coil, which discharges the magnet current. Note that these results can be directly extended to a twin-aperture magnet protected by two identical CLIQ units triggered simultaneously, as explained in [19], [27].

Similar transients are simulated for the four CLIQ configurations shown in Fig. 2 over a range of initial currents

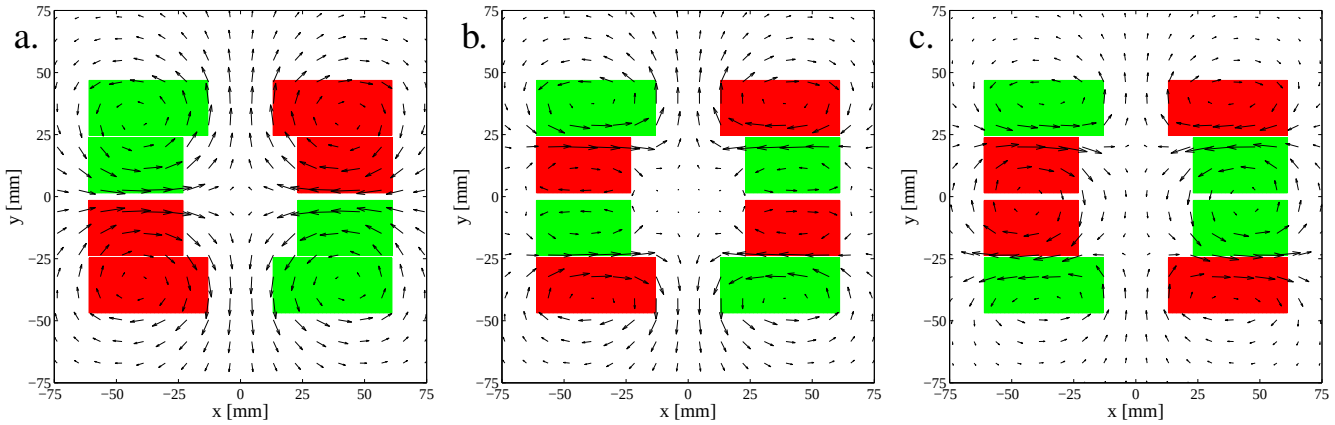


Fig. 3. CLIQ configurations applied to a block-coil dipole magnet. Polarities of the current changes introduced by CLIQ and directions of the introduced magnetic-field changes. a. Pole-Pole. b. Crossed-Layer. c. Layer-Layer.

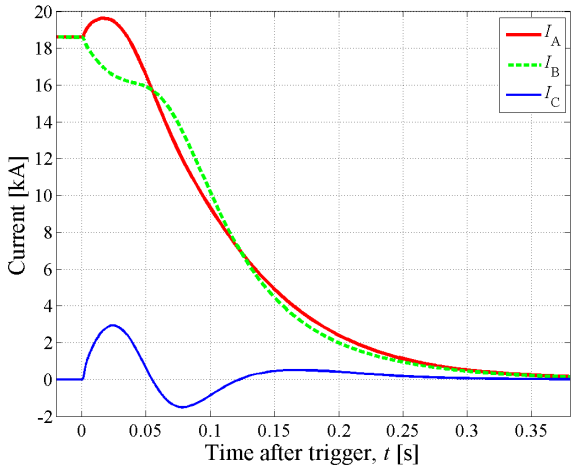


Fig. 4. Discharge of the 14 m long, 16 T, "Coil A" magnet by means of a 100 mF, 1 kV, Pole-Pole CLIQ system. Simulated currents $I_{\mathrm{A}}$, $I_{\mathrm{B}}$, and $I_{\mathrm{C}}$, versus initial current.

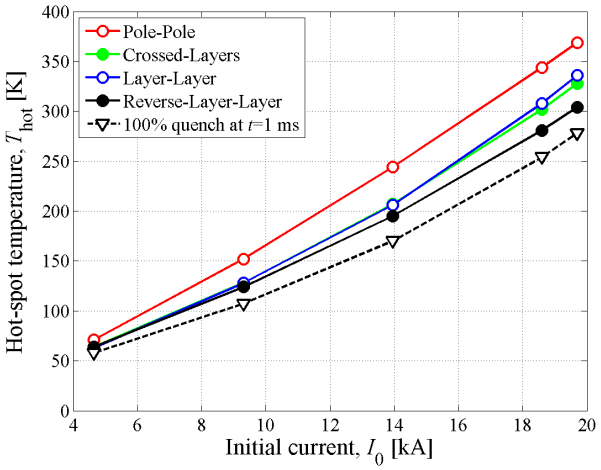


Fig. 5. Performance of a 100 mF, 1 kV CLIQ system applied to the 14 m long block-coil dipole magnet (Coil A). Simulated hot-spot temperature $T_{\mathrm{hot}}$ versus initial current.

from 4 to 20 kA, covering the operating range of interest. The temperatures in the coil's hot-spot at the end of the discharges $T_{\mathrm{hot}}$ [K] are plotted in Fig. 5. The calculation is performed for a quench occurring in the coil's highest magnetic-field region, assuming adiabatic conditions, a 15 ms delay for quench detection and validation, and 1 ms delay for triggering the CLIQ unit. All configurations feature a monotonic increase of $T_{\mathrm{hot}}$ for increasing current levels, and up to the nominal current they can maintain $T_{\mathrm{hot}}$ below the value of 350 K, currently assumed to be an acceptable upper limit with respect to permanent magnet degradation [33].

As expected, configurations including intra-layer terminals achieve better performance with respect to Pole-Pole, resulting in a reduction of $T_{\mathrm{hot}}$ between 50 and 75 K at nominal current. Configuration Reverse-Layer-Layer features the lowest $T_{\mathrm{hot}}$, just 25 K above the value that could be achieved with an ideal protection system instantaneously transferring the entire winding pack to the normal state.

## III. Magnet and Conductor Design Optimization

With CLIQ, a quench protection system capable to turn most of the coil to the normal state in a few tens of millisecond is available to the magnet-designer community. Including CLIQ-optimization studies from the beginning of the design will fully exploit the potential of CLIQ technology by investigating and implementing various modifications in the magnet and conductor design. Far from exhausting all design possibilities, this study provides useful guide-lines for selecting magnet features improving CLIQ performance and explores new limits for high energy-density magnet protection.

### A. Coil designs

Four 2-layer, 16 T, block-coil dipole magnet designs alternative to Coil A are examined:

- Coil B, featuring about 20% fewer turns and 20% thicker cable (see Fig. 6a);
- Coil C, featuring about 20% more turns and 20% thinner cable (see Fig. 6b);

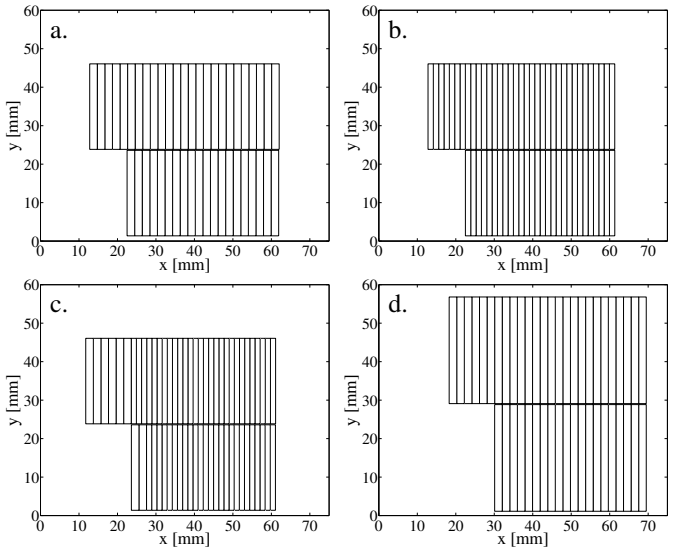


Fig. 6. Cross-sections of one quadrant of the four proposed variants of the 16 T block-coil dipole magnet [28]. a. Coil B. b. Coil C. c. Coil D. d. Coil E.

TABLE II
MAIN MAGNET PARAMETERS OF THE ANALYZED VARIANTS [28].

| Coil | $N_{\mathrm{T}}$ | $I_{\mathrm{nom}}$ [kA] | $L'$ [mH/m] | $f_{\mathrm{d}}$ [mT/kA] | $f_{\mathrm{p}}$ [mT/kA] |
|---|---|---|---|---|---|
| A | 54 | 18.6 | 6.42 | 860 | 910 |
| B | 45 | 22.5 | 4.41 | 710 | 752 |
| C | 63 | 16.1 | 8.73 | 992 | 1038 |
| $\mathrm{D_{in}}$ | 8 | 17.1 | 8.50 | 938 | 979 |
| $\mathrm{D_{out}}$ | 53 | | | | 864 |
| E | 46 | 26.3 | 5.14 | 608 | 652 |

TABLE III
MAIN CONDUCTOR PARAMETERS OF THE ANALYZED VARIANTS [28].

| Coil | $N_{\mathrm{S}}$ | $d_{\mathrm{s}}$ [mm] | $w$ [mm] | $h$ [mm] | $J_{\mathrm{sc}}$ [kA/mm$^2$] |
|---|---|---|---|---|---|
| A | 51 | 0.80 | 22.0 | 1.40 | 1.32 |
| B | 41 | 1.00 | 22.0 | 1.75 | 1.27 |
| C | 61 | 0.67 | 22.0 | 1.39 | 1.36 |
| $\mathrm{D_{in}}$ | 41 | 1.00 | 22.0 | 1.75 | 0.96 |
| $\mathrm{D_{out}}$ | 64 | 0.64 | 22.0 | 1.12 | 1.51 |
| E | 51 | 1.00 | 27.5 | 1.75 | 1.20 |

- Coil D, featuring the graded coil design proposed in [10] (see Fig. 6c);
- Coil E, featuring an increase of the aperture from 40 to 55 mm, and 20% thicker and wider cable (see Fig. 6d) [11].

The main magnet and conductor parameters of the alternative designs are summarized and compared to Coil A in Tables II and III, respectively [28].

Coils B and C are designed so as to have an almost identical product between the number of turns $N_{\mathrm{T}}$ and the operating current $I_{\mathrm{nom}}$ with respect to Coil A and thus achieve the target dipole field of 16 T at a similar superconductor current density $J_{\mathrm{sc}}$ [A/m$^2$]. Their dipole fields and peak fields in the coil per unit current, $f_{\mathrm{d}}$ [T/A] and $f_{\mathrm{p}}$ [T/A], are roughly proportional to $N_{\mathrm{T}}$. Their cable widths $w$ [m] are kept constant, and the cable heights $h$ [m], strand numbers $N_{\mathrm{S}}$ and strand diameters $d_{\mathrm{s}}$ [m] are adjusted to meet the previous constraints. In the first approximation, their self-inductances per unit length $L'$ [H/m] are proportional to the square of $N_{\mathrm{T}}$.

Manufacturing Coils B and C pose some concerns. Winding the thicker, more rigid cable of Coil B with the same bending radius of Coil A may prove more difficult. The conductor of Coil C may prove less stable due to its high aspect ratio.

The graded Coil D features different current densities in its series-connected insert and outsert, optimized as a function of the cable magnetic-field to reach similar margin to quench in operating conditions [10]. Coil D presents several aspects which make it more difficult to build. Since its insert and outsert feature cables with dimensions similar to Coil B and C, respectively, manufacturing Coil D is expected to face the same challenges outlined in the previous paragraph. Furthermore, Coil D design assumes no spacer between insert and outsert in order to maximize its magnetic efficiency, which would require to wind, react and impregnate them together. This process may prove problematic [10].

Coils A, B, C and D occupy the same envelope and have the same iron yoke, whereas the strand area of Coil E is increased by 33%. This coil is less compact than the others and features a lower current density [11]. Its manufacture represents a relatively simple scale-up design and does not seem to pose any significant challenge with respect to Coil A.

### *B. Thermal analysis*

The fraction of non-copper $f_{\mathrm{nonCu}}$ is a key parameter while designing the magnet. Higher $f_{\mathrm{nonCu}}$ is preferable to design a more compact and cost-effective coil. The short sample performance improvement obtained by increasing the non-copper fraction from 0.4 to 0.6 is equivalent to the one obtained assuming a 50% higher critical current density in the superconductor. However, reducing the copper fraction makes the quench protection more challenging.

Thus, the influence of $f_{\mathrm{nonCu}}$ on the magnet protection has to be accurately assessed to select a good compromise value between magnetic performance and quench protection. In this analysis, to provide a suitable margin on the coil's hot-spot temperature, a value of $T_{\mathrm{hot}}$=300 K over the allowed operating range is targeted.

As shown in Fig. 5, given the coil's high energy-density and the relatively low margin to quench, the most critical condition from the thermal point of view is constituted by a magnet discharge from nominal current. Note that the case of a discharge at short-sample current is less relevant for quench protection, since special quench detection conditions can be set for this particular type of test. For each analyzed coil design, two sets of CLIQ discharges at $I_{\mathrm{nom}}$ are simulated: one featuring the Pole-Pole configuration, which is the easiest to manufacture, and the other featuring the Reverse-Layer-Layer configuration, which maintains the hot-spot temperature to the lowest level.

The $T_{\mathrm{hot}}$ obtained for the Pole-Pole case are plotted in Fig. 7. The hot-spot temperature can be maintained below 300 K only by reducing $f_{\mathrm{nonCu}}$ to some 50% in Coils B and E, and to some 45% in Coils A and C. Coil D cannot be effectively protected by this Pole-Pole configuration.

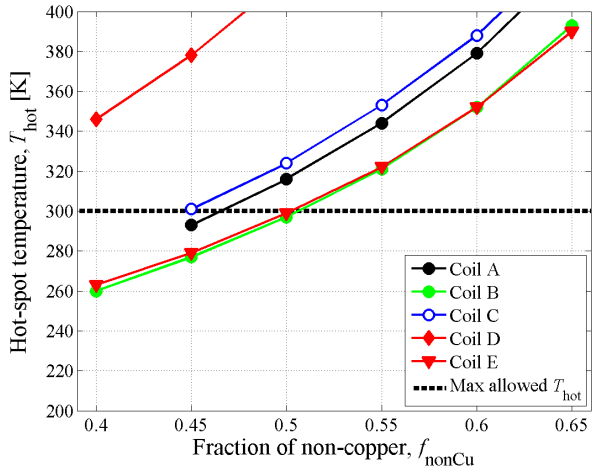


Fig. 7. Performance of a 100 mF, 1 kV, Pole-Pole CLIQ system applied to the reference coil (Coil A) and to various proposed coils (Coils B-E). Simulated hot-spot temperature $T_{\rm hot}$ versus fraction of non-copper in the conductor.

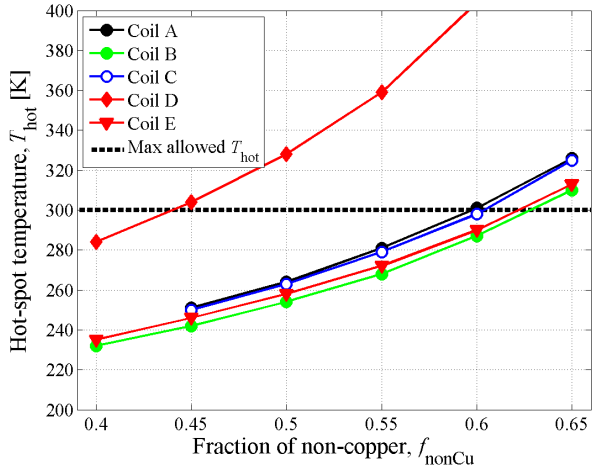


Fig. 8. Performance of a 100 mF, 1 kV, Reverse-Layer-Layer CLIQ system applied to the reference coil (Coil A) and to various proposed coils (Coils B-E). Simulated hot-spot temperature $T_{\rm hot}$ versus fraction of non-copper in the conductor.

The hot-spot temperatures obtained for the CLIQ Reverse-Layer-Layer configuration are plotted in Fig. 8. Due to the significant reduction of $T_{\rm hot}$ achieved by this optimized configuration, the fraction of non-copper can be substantially increased to some 60% to 63% without surpassing the maximum allowed $T_{\rm hot}$, for all coil designs but Coil D. In the graded coil design, the condition on $T_{\rm hot}$ can be met only by reducing $f_{\rm nonCu}$ to 44%.

### C. Quench margin

The baseline magnet design, featuring Coil A and $f_{\rm nonCu}$=55% and named hereafter "Coil A0", does not provide sufficient operating margin for operation at 16 T with currently available conductor [10]. When operating at a dipole field of 16 T, the temperature margin to quench $T_{\rm mq}$ [K] is less than 1.9 K, corresponding to an enthalpy to quench $E_{\rm mq}$ [J/m$^3$] of about 4.5 mJ/cm$^3$, which is less than comfortable for long-term operation. Besides, the ratio between operating and critical current $I_{\rm nom}/I_{\rm c}$ is as high as 75%, and between operating and short-sample current $I_{\rm nom}/I_{\rm ss}$ is 94%. These quench margin parameters are summarized in Table IV.

TABLE IV
QUENCH MARGIN FOR THE BASELINE DESIGN AND FOR ALTERNATIVE DESIGNS WITH HOT-SPOT TEMPERATURE LOWER THAN 300 K.

| Coil | $f_{\rm nonCu}$ | $T_{\rm mq}$ [K] | $E_{\rm mq}$ [mJ/cm$^3$] | $I_{\rm nom}/I_{\rm c}$ | $I_{\rm nom}/I_{\rm ss}$ |
|---|---|---|---|---|---|
| A0 | 0.550 | 1.86 | 4.53 | 0.746 | 0.940 |
| A | 0.597 | 2.22 | 6.44 | 0.687 | 0.925 |
| B | 0.628 | 2.54 | 8.17 | 0.633 | 0.911 |
| C | 0.604 | 2.33 | 6.61 | 0.676 | 0.921 |
| D | 0.440 | 2.50 | 6.44 | 0.694 | 0.913 |
| E | 0.622 | 2.52 | 8.10 | 0.628 | 0.912 |

The implementation of a CLIQ-based protection system allows increasing the content of non-copper while still remaining below the safe limit of hot-spot temperature of 300 K. For instance, an increase of the non-copper fraction to some 60% increases the temperature margin of Coil A by 0.5 K and its enthalpy margin by almost 50%. For each analyzed coil design, the highest allowed values of $f_{\rm nonCu}$, deduced from Fig. 8, are reported in Table IV, together with the respective quench-margin parameters.

The designs assuring the highest quench margins are Coils B and E, whose $E_{\rm mq}$ is almost twice than Coil A0. In these cases, $I_{\rm nom}/I_{\rm c}$=69% and $I_{\rm nom}/I_{\rm ss}$=91%. The enthalpy margins achieved with the other Coils A, C and D are about 50% higher than Coil A0. In this way, the CLIQ system allows exploring more efficient design options while significantly reducing the demands on conductor improvements in order to achieve a sufficient margin for operation at 16 T.

The fraction of non-copper is treated here as a free parameter. However, too small a copper fraction may cause high magnetic-field instabilities and increase the risk of damaging the strands during the cabling process. Additional studies are under way, analogous to the studies of the effect of RRR on the magnet stability [34].

### D. Electrical analysis

The peak voltages developed during and after a CLIQ discharge are analyzed. The relatively high charging voltages imposed by CLIQ across the various coil sections, the very fast rise of resistive voltages, and the high inductive voltages due to the fast magnet discharge can result in significant voltage build-up. The electrical order of the coil sections was optimized for each CLIQ configuration and coil design [28].

Figure 9 shows the simulated distribution of the voltages to ground in the coil windings, at 90 ms after triggering a Reverse-Layer-Layer CLIQ discharge at nominal current. At this moment, the peak coil-to-ground voltages are reached. The turns reaching the highest voltages to ground ($\pm$1.2 kV) are located around the electrical center of the inner layers.

Various characteristic voltages are identified, which may prove critical for the magnet safety and may require an increase of the thickness of the insulation layers: the voltage between the coil and its mechanical support structure $U_{\rm CS}$ [V];

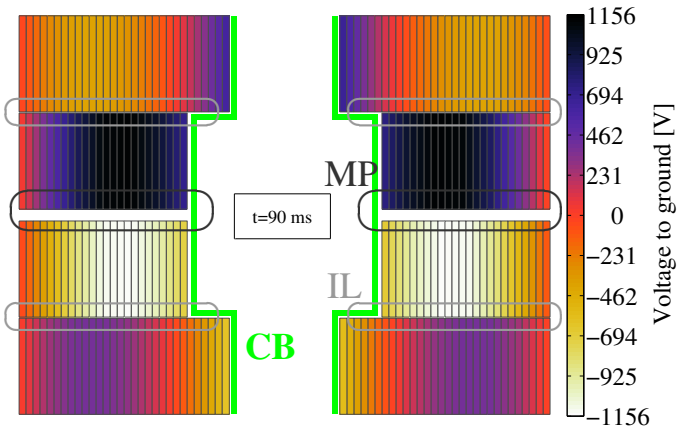


Fig. 9. Simulated distribution of the voltage to ground in the coil windings, at 90 ms after triggering a Reverse-Layer-Layer CLIQ at nominal current (Coil A, $C$=100 mF, $U_0$=1 kV). The characteristic voltages reported in Table V are highlighted.

TABLE V
PEAK CHARACTERISTIC VOLTAGES DEVELOPED DURING A REVERSE-LAYER-LAYER CLIQ DISCHARGE, IN UNITS OF KV [28].

| Coil | $U_{\mathrm{CS}}$ | $U_{\mathrm{CB}}$ | $U_{\mathrm{IL}}$ | $U_{\mathrm{MP}}$ | $U_{\mathrm{TT}}$ |
|---|---|---|---|---|---|
| A | 0.7 | 0.7 | 1.6 | 2.3 | 0.055 |
| B | 0.9 | 0.6 | 1.1 | 1.8 | 0.055 |
| C | 0.6 | 0.8 | 2.0 | 2.9 | 0.065 |
| D | 0.8 | 0.4 | 1.6 | 2.4 | 0.170 |
| E | 0.6 | 0.7 | 1.3 | 1.9 | 0.055 |

the voltage between the coil and the inner bore $U_{\mathrm{CB}}$ [V]; the voltage between adjacent layers $U_{\mathrm{IL}}$ [V]; the voltage between mid-plane sections $U_{\mathrm{MP}}$ [V]; the turn-to-turn voltage $U_{\mathrm{TT}}$ [V].

The simulated peak characteristic voltages developed during a Reverse-Layer-Layer CLIQ discharge, for each analyzed coil design, are reported in Table V. For all designs, the voltages between coil and its support structure or the bore are maintained below 900 V, which is deemed a safe level for an insulation thickness in the order of a hundred micrometer, often adopted while designing accelerator magnets. The peak mid-plane voltages range from 1.8 kV for Coil B to 2.9 kV for Coil C, showing a dependence on the coil's self-inductance. Although in absolute terms these voltages reach high levels, one has to consider that the block-coil dipole design features a gap of several millimeter between the mid-planes, which effectively separates them.

In all configurations but Coil D the peak turn-to-turn voltage is comprised between 55 and 65 V. The higher value reached in the Coil D design occurs at the interface between insert and outsert, and therefore does not seem critical.

The inter-layer voltages pose the greatest concerns, since an increase of the insulation thickness between layers would be detrimental to achieving the accurate conductor positioning required to control field quality. Coils B and E reach the lowest $U_{\mathrm{IL}}$ due to their reduced self-inductances, whereas Coil C the highest (2.0 kV).

In conclusion peak voltages internal to the coil are within acceptable limits for any of the analyzed designs, provided the electrical order of the coil sections is correctly optimized.

### *E. Discussion*

All analyzed variants of the 16 T block-coil dipole magnet can be effectively protected with a CLIQ system, provided an optimized positioning of the dedicated terminals and electrical order of the magnet layers are chosen. The Reverse-Layer-Layer CLIQ configuration shows particular promise, maintaining the coil's hot-spot temperature to the lowest level.

The amount of copper in the strands can be optimized in order to maximize the magnetic performance. Variants to the coil design decreasing the self-inductances of the coil sections, such as Coils B and E, feature a reduction of the hot-spot temperature and of the characteristic voltages developed in the coil. Thus, for any given set of thermal and electrical safety margins, these coils can be operated with higher margin to quench. The drawback of these variants is constituted by the high required operating current, 20% and 40% higher than the baseline for the designs B and E, respectively. In fact, all circuit components, such as power supplies and current leads, would need to be rated for these higher current levels, hence increasing their manufacture and operating cost.

Note that Coils B and E achieve similar performances, but the latter, featuring an increased aperture, is significantly less compact than all other proposed designs. The required increase of the coil, iron yoke, and cryostat sizes would lead to a substantial increase of the magnet cost.

The results for the graded Coil D show that in order to limit the hot-spot temperature within safe levels the copper ratio needs to be increased, effectively trading off the potential advantages in terms of achievable margin to quench relative to the baseline design. Therefore, unless a better protection scheme can be developed, the considerable complications of this approach [10] are not justified.

The potential for a significant improvement of the $Nb_3Sn$ superconductor properties, especially in terms of critical current density, has been clearly established in recent years [10], [35]–[37]. Should this be achieved, the coil design could be further improved by increasing the operating margin without any significant impact on the quench protection.

## IV. CONCLUSION AND OUTLOOK

The quench protection of a 16 T, $Nb_3Sn$, block-coil dipole magnet for a 100 TeV Hadron collider with a CLIQ-based system is thoroughly analyzed. CLIQ's more effective heating principle, utilizing transitory losses in the conductor, and more robust electrical design with respect to the conventional technology make it the first choice for protecting this high energy-density coil.

An extensive analysis of the electro-thermal transient following a CLIQ discharge is performed. Various alternative connections of the protection unit to the coil are presented. Reductions of 50 to 75 K of the coil's hot-spot temperature can be achieved by implementing an optimized configuration, which includes inter-layer CLIQ terminals. At nominal current a transition to the normal state can be initiated in less than 5 ms, and after 50 ms most of the coil is quenched.

Alternative block-coil magnet designs are proposed and analyzed, aiming at maximizing the magnetic performance and

the operating margin and minimizing the risks of damage. The choice of the most optimized design is simultaneously affected by many interdependent features and parameters, such as the defined safe limits to hot-spot temperature and coil-to-ground voltages, the selection of the CLIQ configuration, and the conductor parameters, in particular the fraction of copper.

Far from considering all possible design options, the present analysis explores the potential of a CLIQ-based quench protection and provides useful guide lines for optimizing its performance. Design variants featuring decreased self-inductances of the coil sections allow achieving better performance in terms of reduced hot-spot temperature, reduced coil-to-coil and coil-to-ground voltages, and enhanced quench margin. Various coil designs achieving an increase of the energy margin to quench of 50 to 100% with respect to the baseline design are presented.

The invention of CLIQ makes available a quench protection system capable of transferring most of the coil to the normal state in only a few tens of millisecond. Designers of future high magnetic-field superconducting magnets can exploit this remarkable feature, which significantly extends the range of allowed operating parameters.

## REFERENCES


[1] M.J. Syphers, M.A. Harrison, and S. Peggs, "Beyond the LHC: a conceptual approach to a future high energy hadron collider", *Proceedings of the 1995 Particle Accelerator Conference,* vol. 1, May 1995, doi: 10.1109/PAC.1995.504681.

[2] G. Dugan, P. Limon, and M. Syphers, "Really Large Hadron Collider Working Group Summary", *Proceedings of the 1997 DPF/DPB Summer Study on New Directions for High Energy Physics,* Snowmass, 1996, p. 251.

[3] G. Ambrosio *et al.*, "Design Study for a Staged Very Large Hadron Collider", Fermilab TM-2149, June 2001.

[4] R. Assmann *et al.*, "First Thoughts on a Higher-Energy LHC", CERN-ATS-2010-177, 2010.

[5] O. Brüning *et al.*, "High Energy LHC Document prepared for the European HEP strategy update", CERN ATS 2012-237, August 2012.

[6] M. Benedikt, "Future Circular Collider (FCC) Study", *Future Circular Collider Study Kickoff Meeting,* 2014.

[7] L. Bottura, G. de Rijk, L. Rossi, and E. Todesco, "Advanced Accelerator Magnets for Upgrading the LHC", *IEEE Trans. Appl. Supercond.*, vol. 22, no. 3, June 2012, doi: 10.1109/TASC.2012.2186109.

[8] E. Todesco, L. Bottura, G. de Rijk, and L. Rossi, "Dipoles for High-Energy LHC", *IEEE Trans. Appl. Supercond.*, vol. 24, no. 3, June 2014, doi: 10.1109/TASC.2013.2286002.

[9] L. Rossi and E. Todesco, "Conceptual design of 20 T dipoles for High-Energy LHC", CERN Yellow Report 2011-003 13-9, 2011.

[10] G. Sabbi *et al.*, "Performance characteristics of $Nb_3S$ block-coil dipoles for a 100 TeV hadron collider", *IEEE Trans. Appl. Supercond.*, vol. 25, no. 3, June 2015, doi: 10.1109/TASC.2014.2365471.

[11] G. Sabbi *et al.*, "Design Study of a 16 Tesla Block-Dipole for FCC", *IEEE Trans. Appl. Supercond.*, submitted for publication.

[12] L. Rossi and E. Todesco, "Electromagnetic Efficiency of Block Design in Superconducting Dipoles", *IEEE Trans. Appl. Supercond.*, vol. 19, no. 3, June 2009, doi: 10.1109/TASC.2009.2017891.

[13] G. Sabbi *et al.*, "Design of HD2: a 15 tesla $Nb_3S$ dipole with a 35 mm bore", *IEEE Trans. Appl. Supercond.*, vol. 15, no. 2, June 2005, doi: 10.1109/TASC.2005.849510.

[14] P. Ferracin *et al.*, "Mechanical Design of HD2, a 15 T $Nb_3S$ Dipole Magnet with a 35 mm Bore", *IEEE Trans. Appl. Supercond.*, vol. 16, no. 2, June 2006, doi: 10.1109/TASC.2006.871323.

[15] P. Ferracin *et al.*, "Development of the 15 T $Nb_3S$ Dipole HD2", *IEEE Trans. Appl. Supercond.*, vol. 18, no. 2, June 2008, doi: 10.1109/TASC.2008.922303.

[16] P. Ferracin *et al.*, "Assembly and Test of HD2, a 36 mm Bore High Field $Nb_3S$ Dipole Magnet", *IEEE Trans. Appl. Supercond.*, vol. 19, no. 3, June 2009, doi: 10.1109/TASC.2009.2019248.

[17] P. Ferracin *et al.*, "Recent Test Results of the High Field $Nb_3S$ Dipole Magnet HD2", *IEEE Trans. Appl. Supercond.*, vol. 20, no. 3, June 2010, doi: 10.1109/TASC.2010.2042046.

[18] D.W. Cheng *et al.*, "Design and Fabrication Experience With $Nb_3S$ Block-Type Coils for High Field Accelerator Dipoles", *IEEE Trans. Appl. Supercond.*, vol. 23, no. 3, June 2013, doi: 10.1109/TASC.2013.2246811.

[19] E. Ravaioli, "CLIQ", PhD thesis University of Twente, The Netherlands, 2015, doi: 10.3990/1.9789036539081.

[20] V.I. Datskov, G. Kirby, and E. Ravaioli, "AC-Current Induced Quench Protection System", EP13174323.9, priority date: 28 June 2013.

[21] E. Ravaioli *et al.*, "New, Coupling Loss Induced, Quench Protection System for Superconducting Accelerator Magnets", *IEEE Trans. Appl. Supercond.*, vol. 24, no. 3, June 2014, doi: 10.1109/TASC.2013.2281223.

[22] E. Ravaioli *et al.*, "First Experience with the New Coupling-Loss Induced Quench System", *Cryogenics*, 2014, Vol. 60, pp. 33-43, http://dx.doi.org/10.1016/j.cryogenics.2014.01.008.

[23] E. Ravaioli, V.I. Datskov, G. Kirby, H.H.J. ten Kate, and A.P. Verweij, "A New Hybrid Protection System for High-Field Superconducting Magnets", *Superconductor Science and Technology*, 2014, Vol. 27 (4), 044023, doi: 10.1088/0953-2048/27/4/044023.

[24] E. Ravaioli *et al.*, "Protecting a Full-Scale $Nb_3Sn$ Magnet with CLIQ, the New Coupling-Loss Induced Quench System", *IEEE Trans. Appl. Supercond.*, vol. 25, no. 3, June 2015, doi: 10.1109/TASC.2014.2364892.

[25] E. Ravaioli *et al.*, "Towards an optimized Coupling-Loss Induced Quench protection system (CLIQ) for quadrupole magnets", *Physics Procedia*, Vol. 67, Pages 215-220, ISSN 1875-3892, 2015, doi: 10.1016/j.phpro.2015.06.037.

[26] E. Ravaioli *et al.*, "First implementation of the CLIQ quench protection system on a full-scale accelerator quadrupole magnet", *IEEE Trans. Appl. Supercond.*, vol. 26, no. 3, 2015, doi: 10.1109/TASC.2016.2529840.

[27] E. Ravaioli *et al.*, "First Implementation of the CLIQ Quench Protection System on a 14 m Long Full-scale LHC Dipole Magnet", *IEEE Trans. Appl. Supercond.*, vol. 26, no. 3, 2015, doi: 10.1109/TASC.2015.2510400.

[28] J. Blomberg Ghini, "CLIQ Based Quench Protection of 16 T $Nb_3Sn$ BlockCoil Dipole Magnets for a Future Circular Collider", Master's thesis, CERN, 2015.

[29] E. Ravaioli, B. Auchmann, M. Maciejewski, H.H.J. ten Kate, and A.P. Verweij, "Lumped-Element Dynamic Electro-Thermal model of a superconducting magnet", *Cryogenics*, 2015, submitted for publication.

[30] M. Maciejewski, E Ravaioli, B. Auchmann, A.P. Verweij, and A. Bartoszewicz, "Automated Lumped-Element Simulation Framework for Modelling of Transient Effects in Superconducting Magnets", *Proceedings of the 20th International Conference on Methods and Models in Automation and Robotics*, 2015.

[31] M. Maciejewski, "Automated, Object Oriented Simulation Framework for Superconducting Magnets Modelling at CERN", Master's thesis University of Łodz, Poland, 2014.

[32] A.P. Verweij, "Electrodynamics of Superconducting Cables in Accelerator Magnets", PhD thesis University of Twente, The Netherlands, 1995.

[33] G. Ambrosio, "Maximum allowable temperature during quench in $Nb_3S$ accelerator magnets", *CERN Yellow Report* CERN-2013-006, pp.43-46, 2013, doi: 10.5170/CERN-2013-006.43.

[34] B. Bordini, L. Bottura, L. Oberli, L. Rossi, and E. Takala, "Impact of the Residual Resistivity Ratio on the Stability of $Nb_3Sn$ Magnets," *IEEE Trans. Appl. Supercond.,* vol. 22, no. 3, June 2012, doi: 10.1109/TASC.2011.2180693.

[35] D.R. Dietderich and A. Godeke, "$Nb_3Sn$ research and development in the USA Wires and cables," *Cryogenics* 48 (2008).

[36] X. Xu, M. Sumption, X. Peng, and E.W. Collings, "Refinement of $Nb_3Sn$ grain size by the generation of ZrO2 precipitates in $Nb_3Sn$ wires," *Appl. Phys. Lett.* 104 082602 (4pp).

[37] X. Xu *et al.*, "Refinement of $Nb_3Sn$ grain size by the generation of $ZrO_2$ precipitates application of internal oxidation method in $Nb_3Sn$ wires," *Applied Superconductivity Conference,* Charlotte, NC, August 2014.